GigaScience, 2022, **11**, 1–11
DOI: 10.1093/gigascience/giac075
TECH NOTE

Stardust: improving spatial transcriptomics data analysis through space-aware modularity optimization-based clustering

Simone Avesani [1,†], Eva Viesi [1,†], Luca Alessandrì [2], Giovanni Motterle[1], Vincenzo Bonnici [4], Marco Beccuti [3], Raffaele Calogero [2] and Rosalba Giugno [1,*]

[1]Department of Computer Science, University of Verona, Verona 37134, Italy
[2]Department of Molecular Biotechnology and Health Sciences, University of Turin, Turin 10126, Italy
[3]Department of Computer Science, University of Turin, Turin 10149, Italy
[4]Department of Mathematical, Physical and Computer Sciences, University of Parma, Parma 43121, Italy
*Correspondence address. Rosalba Giugno, Department of Computer Science, University of Verona, Strada le Grazie 15, 37134 Verona, Italy.
E-mail: rosalba.giugno@univr.it
†Equal contributor.

Abstract

Background: Spatial transcriptomics (ST) combines stained tissue images with spatially resolved high-throughput RNA sequencing. The spatial transcriptomic analysis includes challenging tasks like clustering, where a partition among data points (spots) is defined by means of a similarity measure. Improving clustering results is a key factor as clustering affects subsequent downstream analysis. State-of-the-art approaches group data by taking into account transcriptional similarity and some by exploiting spatial information as well. However, it is not yet clear how much the spatial information combined with transcriptomics improves the clustering result.

Results: We propose a new clustering method, *Stardust*, that easily exploits the combination of space and transcriptomic information in the clustering procedure through a manual or fully automatic tuning of algorithm parameters. Moreover, a parameter-free version of the method is also provided where the spatial contribution depends dynamically on the expression distances distribution in the space. We evaluated the proposed methods results by analyzing ST data sets available on the 10x Genomics website and comparing clustering performances with state-of-the-art approaches by measuring the spots' stability in the clusters and their biological coherence. Stability is defined by the tendency of each point to remain clustered with the same neighbors when perturbations are applied.

Conclusions: *Stardust* is an easy-to-use methodology allowing to define how much spatial information should influence clustering on different tissues and achieving more stable results than state-of-the-art approaches.

Keywords: spatial transcriptomics analysis, clustering, stability scores, parameters tuning, software comparison

Background

Single-cell RNA sequencing (scRNA-seq) has emerged as an essential tool to investigate cellular heterogeneity [1]. Individual cells of the same phenotype are commonly viewed as identical functional units of a tissue or an organ. However, single-cell sequencing results suggest the presence of a complex organization of heterogeneous cell states producing together system-level functionalities. Thus, the comprehension of cell transcriptomics in their morphological context is crucial to understand the effect of tissue organization in complex diseases, like specific cancer subtypes [2]. The pioneering technology called spatial transcriptomics (ST) [3–5] is able to preserve spatial information in transcriptomics by integrating the features of microarray and the scRNA-seq barcoding system. In contrast to single-cell sequencing, spatial transcriptomics is only able to sequence the merged transcriptome profile of a small group of cells, also called a spot. By adding spatial information to scRNA-seq data, spatially resolved transcriptomes are reshaping our understanding of tissue functional organization [6]. The progressive increase in the use of ST technology highlights the need for new methods for optimizing the extraction of knowledge from ST data [7–10].

A spatial transcriptomics analysis involves upstream analysis such as data preprocessing, gene imputation and spatial decomposition, and downstream analysis such as spatial clustering, identification of spatially variable genes, and gene–cell interactions. The technology is continuously evolving, raising significant challenges on the above workflow in all different steps; however, downstream analysis tends to be technology agnostic. Among all the emerging contributions in this young research area, several tools can be considered state of the art, mainly focused on downstream cluster analysis of ST data [11–14]. Pham et al. [11] presented *stLearn* to perform downstream analysis and cell-type development states identification by integrating tissue morphology, spatial dimensionality, and the transcriptional information extracted from the cells. *stLearn* uses a deep neural network model to perform tile-based feature extraction from high-resolution histology images. The extracted morphological features, together with the expression value of the neighboring spots, are exploited to

Received: December 14, 2021. **Revised:** April 27, 2022. **Accepted:** June 30, 2022

smooth the gene expression data before the clustering task. Then, *stLearn* applies the Louvain or *k*-means clustering methods to derive the cluster to which each spot belongs. To cluster data, *stLearn* takes as input the number of principal components (PCs), the number of neighbors to build the k-nearest neighbor graph, and the resolution of the clustering algorithm.

In the same year, Hu et al. [12] developed *SpaGCN*, which introduces a data integration approach based on graph convolution. *SpaGCN* as *stLearn* adds the histological information in the clustering task. It represents, through a weighted graph, the gene expression and also the similarity between each pair of spots. The latter is calculated taking into account the spatial coordinates of the spots and the average RGB value in a square of pixels to which the spots belong. The method allows increasing the weight given to histological information by varying the contribution of spots when aggregating gene expression data. To give a higher weight to images with a clear histological structure, the scaling parameter *s* can be increased when calculating the pairwise distance between spots. The hyperparameter *l* (i.e., the characteristic length scale) can be tuned starting from the parameter *p*, which determines the percentage of total expression provided by the neighbors. The characteristic length scale determines the contribution of neighboring spots when aggregating gene expression data by adjusting the edge weight between pairs of spots. Then, *SpaGCN* uses Louvain's method on the aggregated output matrix from graph convolution layers to perform clustering. In addition, this method enables setting the size of the RGB square of pixels, the number of PCs, and the resolution of the clustering algorithm. Moreover, users have the possibility to discard or keep the image information by setting a Boolean flag. *SpaGCN*, as other tools, allows identifying spatially variable genes or meta genes for each resulting spatial domain to give a biological meaning to the detected clusters as reported in Hu et al. [7].

Subsequently, Dries et al. [13] presented *Giotto*, a toolbox of algorithms, including a hidden Markov random field (HMRF) method, to analyze spatial gene expression profiling associated with histological images. *HMRF* is a graph-based model that characterizes how many spots are influenced by the neighbors in order to assign each spot to one of *k* spatial domains (i.e., clusters), where *k* is given in input by the user. In *Giotto*, the parameters to be set are the ones given in input to the *HMRF* function, that is, the expression values to use, the name of the spatial network employed, the spatially variable genes, the spatial dimensions, the name of the dimension reduction method, the number of PCs, the number of spatial domains (or clusters), and three parameters (beta, tolerance, and z score) for the initialization of the method. Differently from the above methods, *Giotto* uses only spatial information of the spots and not histological information.

The same direction of *Giotto* is followed in Zhao et al. [14], who proposed a method, called *BayesSpace*, based on a Bayesian statistical approach, that improves the identification of specific profiles in tissues by imposing a Markov random field prior that gives higher weight to spots that are spatially close. It takes as input the number of PCs and clusters, the spatial transcriptomic platform, and a series of model parameters comprising the initial cluster assignments for spots or the method to obtain the initial assignments, the error model, the precision covariance structure, the number of Markov chain Monte Carlo iterations, the gamma smoothing parameter, the prior mean hyperparameter, the prior precision hyperparameter, and the hyperparameters for Wishart distributed precision. *BayesSpace* allows to cluster the spots according to some *a priori* biological knowledge or otherwise using the elbow plot of the pseudo-log-likelihood to infer the number of clusters *q* that are given in input to the method. The authors show that *BayesSpace* outperforms, in terms of adjusted Rand index and manual annotations, other methods in the literature, in particular, the three widely used nonspatial algorithms, namely, *k*-means, mclust, and Louvain's methods, and the two spatial clustering algorithms, *HMRF* (*Giotto*) and *stLearn*, on distinct samples of a dorsolateral prefrontal cortex data set. This data set was not analyzed in our comparisons due to the lack of publicly available reference manual annotation.

In this article, we propose a downstream ST cluster method, called *Stardust*, which takes into account both the expression and the physical location in the tissue section of the transcriptional profiles, to define the similarity of the objects to be grouped. Our proposed method fits on the downstream task to perform clustering on gene count and spot location matrices. With *Stardust*, we intend to investigate how much the spatial information combined with transcriptomics improves the clustering results. *Stardust* is based on the *Seurat* [15] algorithm for the clustering of scRNA-seq data, which uses Louvain's method to perform clustering. By setting a parameter, the user can easily determine how much spatial information should affect the clustering similarity. Such a parameter can also be automatically derived from a tuning procedure. Moreover, we propose a version of *Stardust* that is parameter free, *Stardust** (i.e., it uses a dynamic nonlinear formulation that changes the spatial weight according to the transcriptomics values in the surrounding space). Running time of the two methods is equivalent.

To understand how the usage of spatial information affects the stability of clusters, we evaluated both *Stardust* approaches with and without considering space on five publicly available 10x Genomics Visium data sets, respectively derived from human breast cancer section 1 (HBC1) and section 2 (HBC2), mouse kidney (MK), human heart (HH), and human lymph node (HLN) tissues [16]. We investigated the scalability of *Stardust**, testing it also on Seq-scope and Slide-seq data sets [17, 18], which provide higher resolution and number of captured cells with respect to Visium data sets that combine spatial information on a tissue section with whole transcriptome sequencing at a resolution of 55 μm. In Seq-scope, two sequencing steps are performed respectively, allowing to retrieve spatial coordinate and captured complementary DNA information. We analyzed two gastrointestinal tissues, liver and colon, for which the sequencing data were produced in 1-mm-wide circular areas called "tiles," achieving a submicrometer resolution (0.5–1 μm). As for Slide-seq, we analyzed the new Slide-seq V2 mouse cerebellum data set, which consists of spatially resolved expression data at approximate resolution of a single cell (10 μm).

We compared *Stardust* and *Stardust** with currently available ST clustering methods, including *stLearn*, *SpaGCN*, *Giotto*, and *BayesSpace*. Each tool comes with specific parameters to be set by the user. We fully exploited the cluster resolution parameter and used the author-suggested values for all the remaining ones. In order to assess clustering performances, we exploited functional aspects such as spatially variable genes, and alternatively from current contributions, we defined two different objective clustering quality measures: the cell stability score (CSS) [19] and the coefficient of variation. The CSS defines the tendency of a cell or spot to remain clustered with the same group of elements when inducing a perturbation to the data set, for instance, by removing a random set of items, while the coefficient of variation value is derived from the CSS distribution as the ratio of the standard deviation to the mean; thus, a lower coefficient of variation means higher average stability and less variation from the mean. These comparison measures enable us to estimate the clustering stability

of the different configurations and to assess whether considering spatial or morphological information leads to an improvement in terms of stability. By computing Moran's *I* [20] for each gene, we showed that genes with the highest spatial autocorrelation values colocalize in clusters achieved by the proposed methods. Moreover, when cell-type annotation is available, we verified that *Stardust* clustering maintains biological significance, observing that cluster shapes appear consistent with the provided annotation.

Results show that *Stardust* and *Stardust** improve in a statistically significant manner the clustering stability by combining the transcriptional similarity of the spots with their spatial localization in several data sets with respect to *stLearn*, *SpaGCN*, and *Giotto*, and it is comparable with *BayesSpace*. Furthermore, while other methods force spots to form misleading cluster structures, in which neighboring spots are clustered without sensibly sharing their expression profile, the proposed methods appear to be unaffected by such behavior. Finally, unlike other approaches, besides the number of principal components and clustering resolution parameters, *Stardust* requires only one parameter (i.e., the spatial weight) to be set by the user, and *Stardust** does not require any parameter.

Methods

In this section, we introduce the proposed ST cluster approaches and the measures used for evaluating performance. Data sets used for the clustering evaluation were downloaded from the 10x Genomics website [16], respectively derived from two serial sections of human breast cancer (HBC1 and HBC2), MK, HH, and HLN and from the Deep Blue Data platform [21], respectively collected from colon and liver *TD*. These data, together with the Slide-seq V2 cerebellum data set [18], were used to estimate method time scalability. For each 10x data set, we loaded the associated *Seurat* object and extracted the spot coordinates and the expression matrix. In order to reduce memory usage and computation time, we filtered in the data matrices those genes expressed in more than 10 spots. To analyze Seq-scope data, we downloaded the processed RDS data files and selected a single tile for each of the two data sets chosen, specifically, the tile ID 2110 for the colon data set and the tile ID 2117 for the liver *TD* data set. The files containing the digital gene expression matrices and the pixel coordinates within the Slide-seq data set were downloaded from the Single Cell Portal website referenced in Cable et al. [18]. Preprocessed 10x data, software code, and tool documentation are available at https://github.com/InfOmics/stardust/.

Stardust

Stardust is implemented on top of the *Seurat* [15] clustering algorithm. *The Seurat* package is one of the most used software for scRNA-seq data analysis. *Seurat* implements a network-based clustering method called the Louvain algorithm [22], which encodes each element of a data set as a node in a graph. Pairs of nodes are connected according to a pairwise measure of similarity based on the Euclidean distance between transcriptional profiles. Then, the algorithm performs a community detection step over the graph to retrieve the data set partition. In *Stardust*, the distance matrix used in *Seurat* is replaced with a summation of two other matrices representing the transcriptional information and the spatial position of the spots. Additionally, the distance among pairs of nodes is computed on the vectors of the distances of each node to all other nodes. The matrix regarding the transcriptional information is obtained from the pairwise Euclidean distance between transcriptional profiles in PCA space [23]. The matrix regarding the spatial position represents the pairwise spatial Euclidean distance between spots.

Given the distance matrix based on transcriptional profiles, *T*, and the distance matrix based on spot coordinates, *S*, a preliminary linear scaling step is applied to *S* in order to mitigate cases in which one measure overpowers the other. The scaling formula is the following:

$$S' = S * \frac{max(T)}{max(S)} \quad (1)$$

where $max(T)$ and $max(S)$ are the maximum value in the matrices *T* and *S*, respectively.

The user can choose between two different variants of the designed tool, namely, *Stardust* or *Stardust**, for the computation of the final distance matrix *ST*. *Stardust* computes the Louvain edge weights through a linear formulation and requires a fixed *a priori* parameter, while *Stardust** computes the final distances through a nonlinear formulation without any *a priori* parameter to be set.

The first method allows the user to specify a parameter called *spaceWeight*, a real number in [0,1] that defines how much to weigh the space with respect to the transcriptional similarity. By configuring a single parameter, the user can control how much the space-based measure weights on the overall measure. The formula for *ST* is

$$ST = S' * spaceWeight + T \quad (2)$$

The second method first computes the normalized values of the expression distance distribution by applying the following formula:

$$T' = (T - min(T)) \ / \ (max(T) - min(T)) \quad (3)$$

Once *T'* is obtained, the final distance matrix *ST* is computed as a mixture of space and transcript information. The latter is always considered in its integrity, while space information is weighted by the normalized expression distances. The formula for *ST* is

$$ST = S' * T' + T \quad (4)$$

The proposed methodology is very simple and flexible; indeed, it can be incorporated into any existing clustering method. Methods are developed as a standalone R package and can be easily installed from the GitHub repository or used through the dedicated docker image.

Cluster validation

In order to give a quantitative performance evaluation of the clustering obtained, we use three different clustering quality measures: the *cell stability score* (implemented in the rCASC package) [19], the *coefficient of variation*, and *Moran's I* (index) [20]. Finally, we investigate the *statistical validation* of the results.

Cell stability score

rCASC [19] takes as input a spatially resolved transcriptome and a clustering algorithm. It computes for each basic element of the data set a CSS that describes how much each element tends to remain clustered with the same other elements through a series of *n* repetitions of the clustering method on *n* different permutations of the data set. The basic concept of the rCASC notion is that a good clustering should remain stable if a perturbation is applied to the data set. A CSS is a real number in [0,1] associated with each individual spot in a data set and computed running the

following three steps. First, the desired clustering method is applied to the data set, and the cluster identity associated with each object (i.e., each spot in our application) is defined. Then, a subset of objects is removed from the original data set (the percentage of objects is decided by the user) and clustered. This step is repeated n times (n is a user parameter). We decided to set the number of permutations to 80 and to remove at each permutation 10% of the spots. In each of the repetitions, the percentage of spots that remain clustered with a particular spot in that permutation is determined by taking the results obtained in the first step as a reference. This value is stored. Finally, for each spot, it is computed how many times the set of spots clustered with it in each of the repetitions in the second step is equal to the set in the first step. This quantity is divided by the number of repetitions, obtaining the stability score. To reduce the computation time, we set a limit of 4 hours for the computation of the CSS for each tool configuration compared.

Coefficient of variation

To decide which configuration of *Stardust* or *Stardust** was the best performing (based on stability scores) on a particular data set with respect to the one not considering the space, we used the coefficient of variation defined as $\frac{\sigma}{|\mu|}$, where σ is the standard deviation of the distribution of the spot scores and μ is its mean. The lower the coefficient of variation, the better the performances. We also applied this metric to the other compared methods to evaluate the best-performing configuration of each tool.

Spatial autocorrelation of cluster markers

To evaluate the biological coherence of the obtained clusters, we compute genes' spatial autocorrelation by using Moran's I [20]. Moran's I uses both feature locations and feature values simultaneously. Spatial autocorrelation is defined as a territorial cluster of similar marker values. If similar expression values of the genes are spatially localized, there is a positive spatial autocorrelation of the data. On the contrary, a spatial proximity of dissimilar values indicates a negative spatial autocorrelation. Moran's I is defined as

$$I = \frac{n}{W} \frac{\sum_{i=1}^{n} \sum_{j=i}^{n} w_{i,j}\, z_i z_j}{\sum_{i=1}^{n} z_i^2} \quad (5)$$

where z_i is the deviation of the genes from the mean, $w_{i,j}$ is the spatial weight between observations, n is the number of spatial units, and W is the sum of all $w_{i,j}$.

Statistical validation

We provide statistical evidence of the variation of cluster stability achieved by the methods in the following way. Given a data set, we first apply *Stardust* or *Stardust**, obtaining a set of stability scores i. Then, for 100 times, we shuffle the spot coordinates and reapply the method, obtaining 100 sets of stability scores $j_1 \ldots j_{100}$. For each couple (i, j_k)—with k in 1 … 100—we evaluate the Wilcoxon statistical test with the null hypothesis that the distribution i is greater than j_k (i.e., the gain in stability obtained from the original spot coordinates is greater than the gain obtained from shuffled spot coordinates).

Results

In this section, we assess the performance of *Stardust* and *Stardust** on five data sets from 10x Genomics, respectively derived from two serial sections of human breast cancer (HBC1 and HBC2), HH, HLN, and MK (see Fig. 1). The dimensions of data sets are 3.798, 3.987, 4.247, 4.035, and 1.438 spots, respectively. Visually, the data sets show different levels of structures, from high levels such as breast tissues, where we expect to find more well-characterized (i.e., stable) clusters, to low ones as in human heart tissue.

To understand how the usage of spatial information affects the stability of clusters, we computed the *cell stability scores* and evaluated the *coefficient of variation* (CV) of the stability scores (see Cluster validation section) of *Stardust* by varying the clustering resolution and the space weight parameters and *Stardust** by varying only clustering resolution (see Methods section). For *Stardust*, the space weights were set to 0, 0.25, 0.5, 0.75, and 1 and cluster resolution to 0.6, 0.8, and 1. Space weight equals 0 and, when space is not considered, corresponds to comparing *Stardust* with respect to its transcriptomic-only-based approach, here referred with the term *no space* used. Space weight equals 1 means that space and transcripts contribute in the same way.

Results show that the introduction of spatial information (Fig. 2A) reduces the coefficient of variation of each *Stardust* configuration with respect to the configuration where space is not considered. Since setting *Stardust* clustering parameters could be challenging, we also used the R package GenSA [24] solution to estimate the best combination of space weight and clustering resolution, maximizing the average cell stability score. We created a dedicated Docker image where GenSA runs the *Stardust* algorithm several times to tune all the required parameters. Coefficients of variation obtained from tuned parameters are shown in Fig. 2A with violet dots. To limit the computation time, *Stardust* tuning was run for each data set, fixing to 10 the maximum number of GenSA iterations. Despite the low number of iterations, the estimated average cell stability scores are all higher than or comparable with our best results. The achieved CVs confirmed the trends observed from the manual tests, allowing to explore *Stardust* configurations not considered before. Tuning running time varied from 4 to 24 hours, depending on many factors, including the data set size and computational resources. By increasing the size of the data sets or the number of combinations of parameters, GenSA does not scale and therefore it is not straightforwardly applicable on the other ST algorithms that are far more complex than *Stardust* in terms of the entire set of parameters that can be configured. A similar behavior to the one described for *Stardust* is reported for *Stardust** in Fig. 3A, where the dynamic setting of the spatial weight leads to a cluster resolution with an average reduced or comparable coefficient of variation to clustering without considering space.

Figures 2 and 3B show cluster stability improvements. Figure 2B investigates 5 different *Stardust* space weight configurations and keeps the cluster resolution fixed to 0.8 (i.e., it focuses the attention on one of the *cell stability score* distributions tested in Fig. 2A). In all the data sets, space is able to increase the overall stability, and although this behavior is not monotonous with the increase of weight given to the space, different space weights allow to achieve the best scores. Figure 3B shows *Stardust** cluster stability comparing its versions with and without space by varying clustering resolution. The Wilcoxon test (see Cluster validation section) was used to evaluate the significance of the results, confirming that the increase of stability scores is not due to chance.

To complete method evaluation, we compute the percentage of spots becoming stable or unstable. Figure 2C compares one of the best-performing configurations of *Stardust* according to the coefficient of variation values in Fig. 2A with the one not using space information for each data set. Regardless of which threshold is

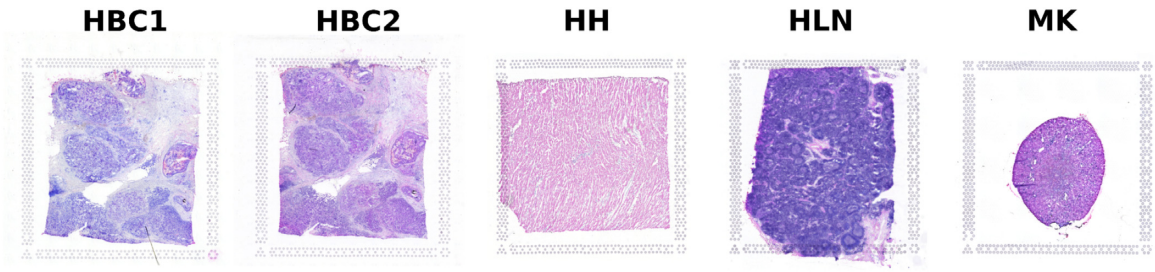

Figure 1: Hematoxylin and eosin (H&E) stained tissue sections of human breast cancer section 1 (HBC1), human breast cancer section 2 (HBC2), mouse kidney (MK), human heart (HH), and human lymph node (HLN).

used, the number of spots that become stable in *Stardust* with respect to the *no space* configuration is always more than the number of spots that become unstable for each data set. However, from a cluster quality point of view, threshold values are reasonable if belonging in [0.5, 1] (i.e., it is desired that each spot remains clustered with the same others in at least half of the rCASC permutations). Using the threshold 0.5, Fig. 3C compares *Stardust** and the same method with *no space* information by varying the clustering resolutions, confirming that besides cluster resolution, the number of spots that become stable using the space information is always more than the number of spots that become unstable for each data set.

In Supplementary Figs. S1–S5, we depict how clusters are arranged in the 2-dimensional space of the tissue section and as space information influences the clusters across the 5 *Stardust* configurations. In Supplementary Figs. S1A–S5A, all points are displayed, while in Supplementary Figs. S1B–S5B, only points with stability scores greater than or equal to 0.5 are displayed. Score values are in [0, 1], so the threshold 0.5 means that in at least half of the permutations, a spot remains clustered with the same other spots and can be considered a stable one. Supplementary Figs. S1 and S2 show that using space, the number of spots that become stable and the number of spots recognized as a unique cluster are maximized without creating structure where it is not present, as in Supplementary Fig. S3. In Supplementary Figs. S4 and S5, spatial information increases the overall stability of neighboring clusters or clusters with distant spots but high transcriptional similarity.

Analyzing clustering results of the most stable configurations, we observed that the cluster structures reflect the biology of the tissue. In Fig. 4A, we report a manual annotation of HBC1 from [2] and the clusters obtained from the most stable configuration of *Stardust**. *Stardust** clustering mirrors the general tissue structure, allowing the identification of tumoral regions, including *ductal carcinoma in situ* regions corresponding to clusters 9 and 12 and *invasive carcinoma* regions like clusters 1, 2, 4, 5, 10, and 11. Moreover, we computed Moran's index for each HBC1 feature to identify spatial autocorrelated genes. Analyzing the first 100 genes with highest Moran's *I*, we noticed that they colocalize in the identified clusters (see Fig. 4B), confirming the biological validity of *Stardust** clustering.

We computed Moran's *I* also for breast cancer (HBC2), MK, HH, and HLN data sets (Supplementary Fig. S6). We observed that, as for HBC1 data set, genes colocalize in well-defined cluster shapes, attesting to the quality of the results achieved by *Stardust**.

Stardust and *Stardust** were also tested and compared with state-of-the-art ST clustering methods, namely, *stLearn*, *SpaGCN*, *Giotto*, and *BayesSpace*, by analyzing each individual 10x Genomics data set. We evaluated *Stardust* stability scores with respect to the ones achieved with the other tools. We fixed the number of principal components to 10, which we found to be a good threshold for all the data sets analyzed through the "*elbow*" method proposed by rCASC [19]. The cluster resolution parameter was set to 0.6, 0.8, and 1 for each tool. For each resolution value, among the 5 configurations of *Stardust* obtained by varying the space weight parameter, we decided to represent the most stable ones, with space weight mainly equal to 0.25 and 0.5 for each data set analyzed. Since *BayesSpace* and *Giotto* require *a priori* knowledge on the number of clusters, we derived it from the results of *Stardust* using for each cluster resolution the *Stardust* configuration with the lowest coefficient of variation score. Moreover, we tested *SpaGCN* both including and excluding histology image information.

Concerning HBC1, by looking at the coefficient of variation in Fig. 5A, *Stardust* and *Stardust** are the tools able to achieve the highest average stability score. Figure 5B shows the stability results of the compared tools, using their best configurations according to Fig. 5A, that is, the ones with the lowest coefficient of variation value: resolution 0.6 and space weight 0.25 for *Stardust*, resolution 0.6 for *Stardust**, resolution 0.6 and image True for *SpaGCN* and *stLearn*, resolution 0.8 for *BayesSpace*, and resolution 0.6 for *Giotto*. *Stardust* and *Stardust** reached the lowest coefficients, followed by *stLearn* and *BayesSpace*. Results for *SpaGCN* with cluster resolution 1 are missing because computation was out of a predefined time (>4 hours). Cluster results for a visual exploration together with the original tissue are shown in Fig. 5C. According to the shifts of the stability scores (Fig. 5D), computed using a threshold of 50%, *Stardust** outperformed all other methods.

Analyzing HBC2, HH, HLN, and MK (Supplementary Figs. S7–S10), we observed that *Stardust* and *Stardust** achieved the lowest values in terms of coefficient of variation (Supplementary Figs. S7A–S10A) and the highest values in terms of average stability (Supplementary Figs. S7B–S10B) overcoming all the other tools. In particular, we noticed that in some cases, only for HBC2, the coefficient of variations were comparable with *BayesSpace* (Supplementary Fig. S7A).

In MK (Supplementary Fig. S10A), *Stardust* and *Stardust** clearly show the lowest coefficient of variation value (Supplementary Fig. S10A) and the highest stability scores, with an average value above 75% (Supplementary Fig. S10B). Supplementary Figs. S7C–S10C graphically show the formed clusters. In HBC2 and MK data sets, *Stardust* and *Stardust** overcame all the other tools in terms of the highest percentage of spots that became stable (Supplementary Figs. S7D and S10D).

Our methods, as well as all the other tools, in tissues such as HH and HLN, characterized by a more homogeneous architecture

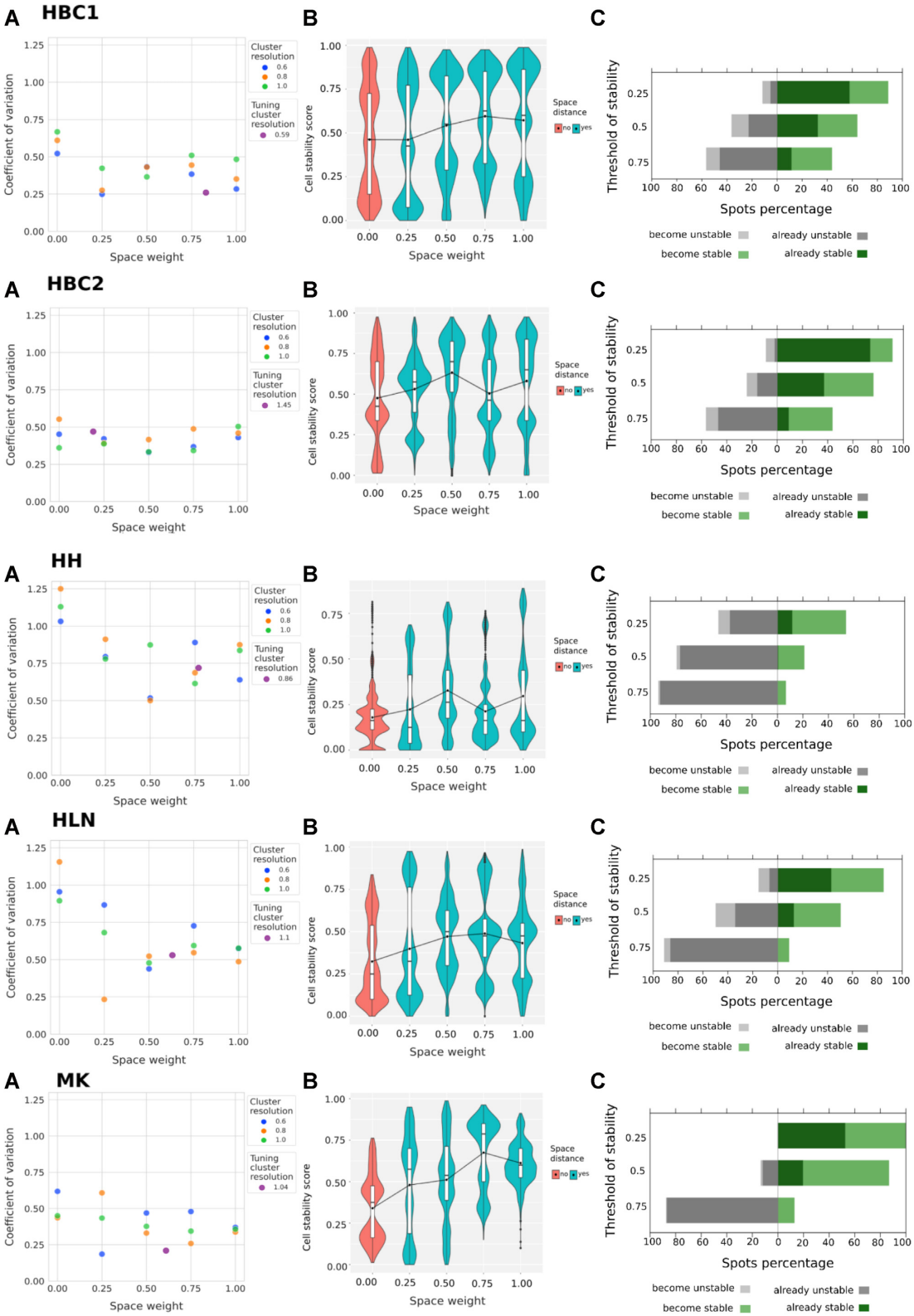

Figure 2: *Stardust* performance on five ST data sets: two sections of human breast cancer (HBC1 and HBC2), mouse kidney (MK), human heart (HH), and human lymph node (HLN). (A) *Stardust* coefficient of variation for each configuration obtained varying the space weight and clustering resolution. Space weight and resolution tuned by maximizing the average cell stability score are shown with violet dots. (B) Stability score comparison for 5 *Stardust* configurations with increasing space weight and cluster resolution fixed to 0.8. (C) The count of spots shifting from stable to unstable and vice versa at stability thresholds equal to 0.25, 0.5, and 0.75, which set the limit to consider a spot stable (above the threshold) or unstable (below the threshold), comparing the best configuration of *Stardust* (i.e., with the lowest coefficient of variation) with the one not using space information.

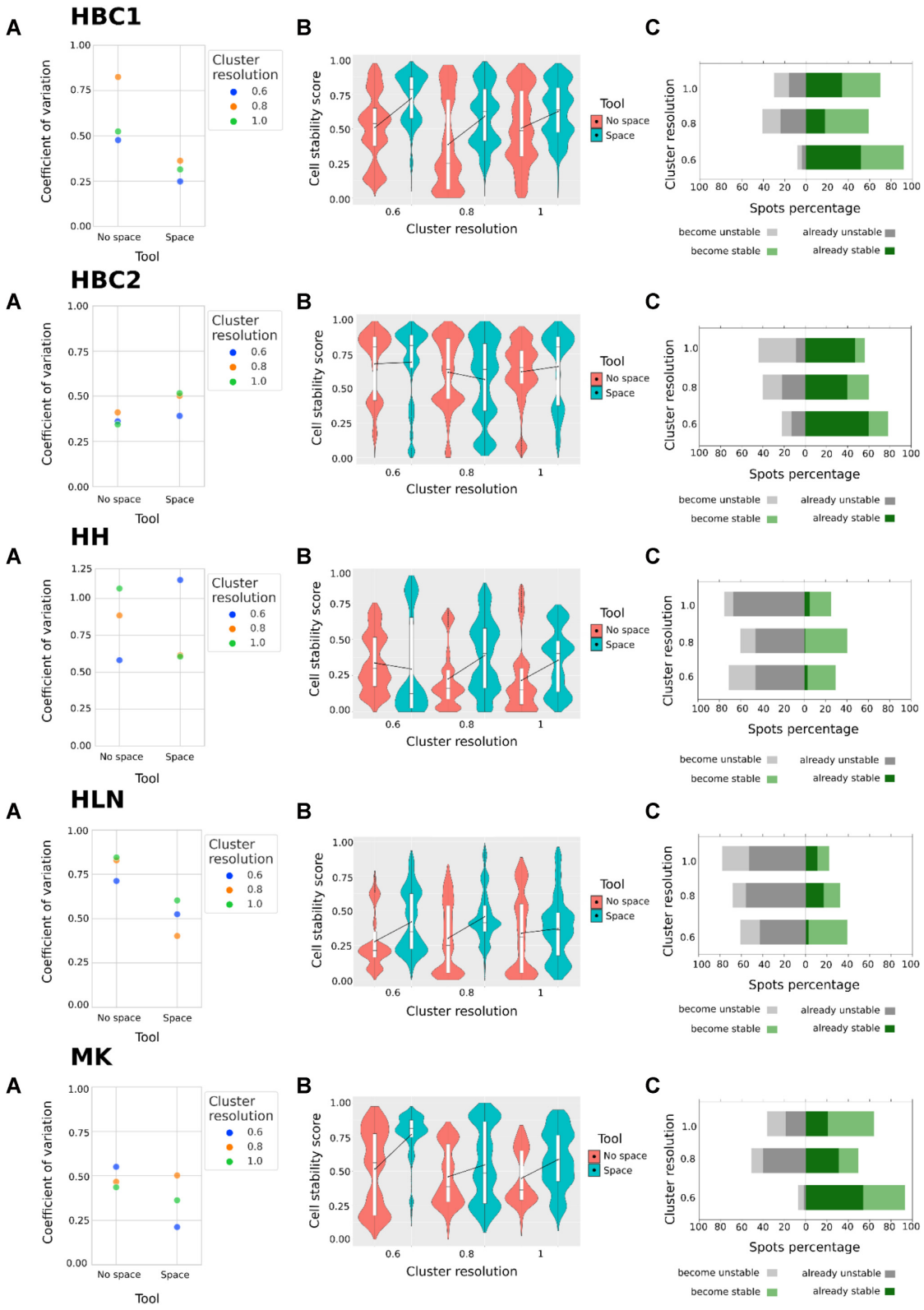

Figure 3: *Stardust** space version performances with respect to *no space* version ones evaluated on 5 ST data sets: 2 serial stages of human breast cancer (HBC1 and HBC2), mouse kidney (MK), human heart (HH), and human lymph node (HLN). (A) Coefficient of variation values comparison for 3 *Stardust** space and *no space* configurations obtained by varying the clustering resolution. (B) Stability scores comparison for 3 *Stardust** *space and no space* configurations obtained by varying the clustering resolution. (C) The *Stardust** count of spots shifting from stable to unstable and vice versa considering clustering with *no space* information as baseline at different clustering resolutions equal to 0.6, 0.8, and 1, which set the limit to consider a spot stable (above the threshold) or unstable (below the threshold).

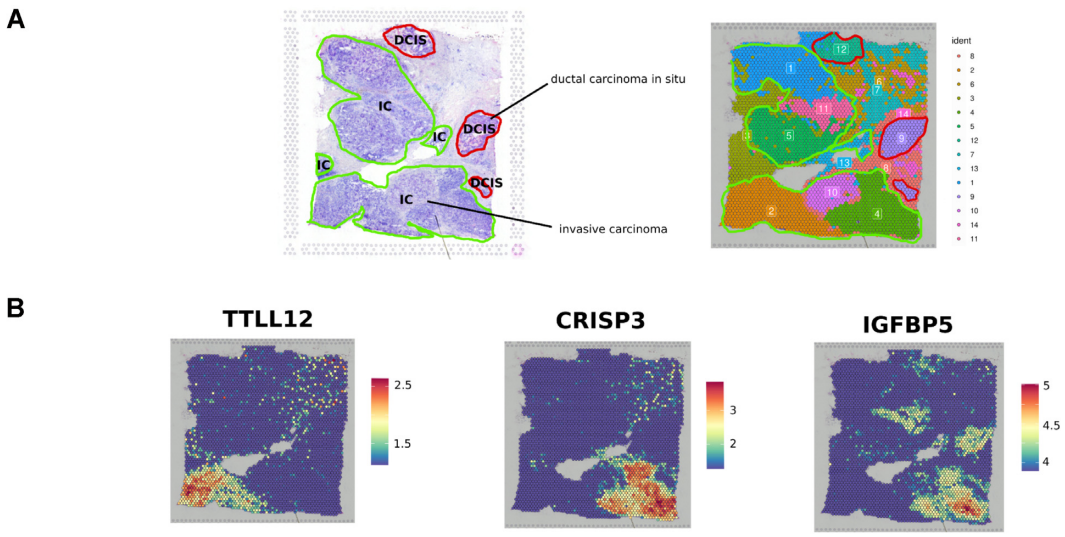

Figure 4: Cluster biological coherence. (A) Manual pathologists' annotation of human breast cancer 1 data set provided by Lewis et al. [2] and clustering achieved with the best configuration of *Stardust** with resolution 0.6. (B) Spatial plots showing the expression level of three of the top 100 genes with highest Moran index for the HBC1 Visium data set.

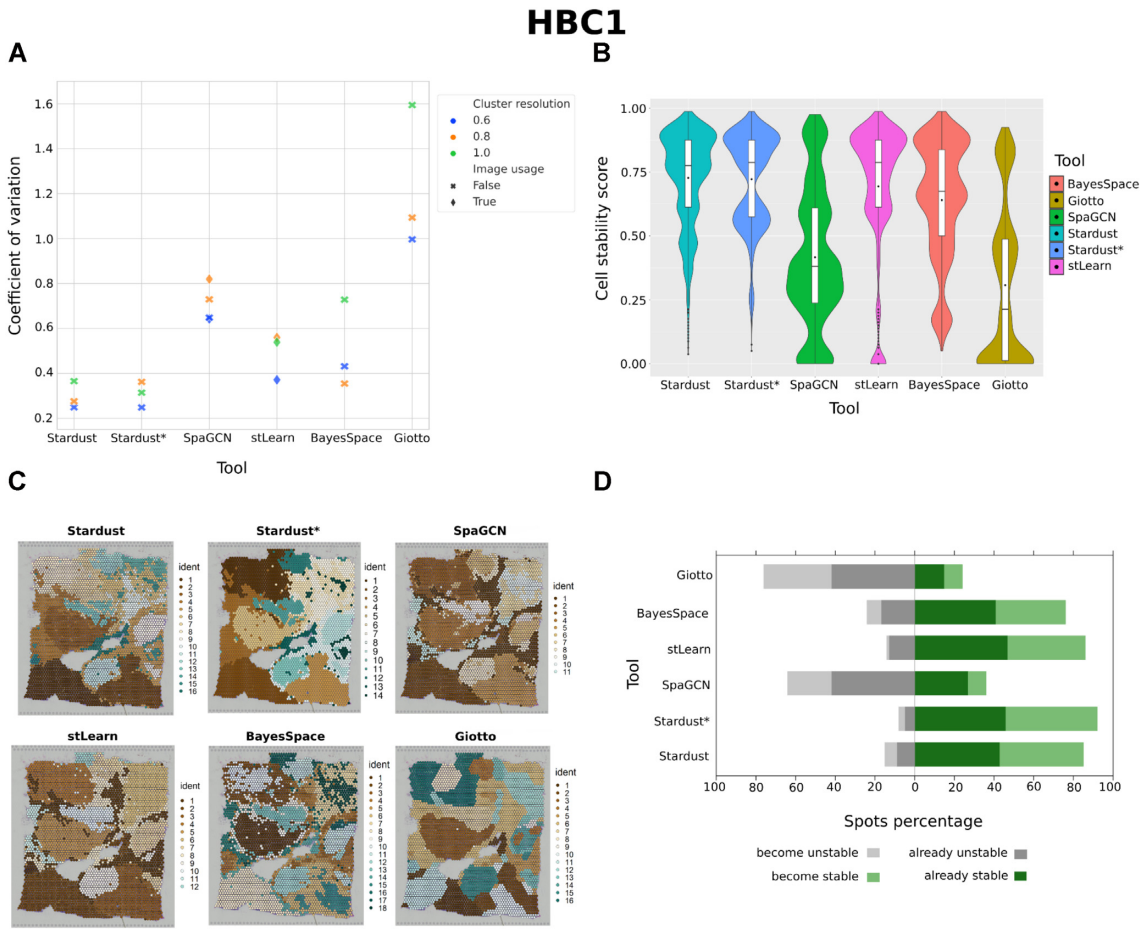

Figure 5: Comparison of *Stardust*, *Stardust**, and state-of-the-art tools on the HBC1 data set. (A) The coefficient of variation values derived from the stability score distribution of each tool configuration. The cluster resolution refers to the resolution parameter for the Louvain community detection algorithm; image usage tells whether the image is included in the clustering method. (B) The cell stability score distributions of the best-performing configuration of each tool (i.e., the one with the lowest coefficient of variation). (C) The hematoxylin and eosin (H&E) stained tissue sample and a spatial plot for each best tool configuration with clusters of spots on the tissue section. (D) The stability score shifts obtained comparing the best configuration of each tool with the base *Stardust no space* version (i.e., the one not considering space).

with respect to the morphological structure clearly visible in the other datasets (Supplementary Figs. S8D and S9D), do not find a relevant number of spots showing a high degree of stability, except for *BayesSpace*, which tends to find a slightly larger number of stable spots.

To show the scalability of *Stardust*, we tested it on the five 10x data sets and on three data sets obtained from two different spatial sequencing technologies, namely, Seq-scope [17] and Slide-seq [18]. Running time of *Stardust** is equivalent to *Stardust*.

Supplementary Fig. S11 shows that the relation between the size of the data set and *Stardust* running time increases linearly. Although the observed relation between the dataset size and the running time is linear, computational resources required for high-dimensional data, such as those generated by Slide-seq technology, consistently increment when using Stardust for clustering.

Quality of *Stardust** clustering was also confirmed by analyzing the biological consistency of the clusters in Seq-scope and Slide-seq data sets (Supplementary Figs. S12–S14) with the available cell annotations and by showing that features with the highest Moran's *I* colocalize inside cluster shapes.

Conclusion

We developed *Stardust*, an open-source and easy-to-install R package for ST data clustering, which integrates transcriptional and spatial information through a complete auto-tuned approach. The package contains a method to manually explore the space influence on clustering (named as the package, *Stardust*) and one version fully automated called *Stardust**. The tools' performances were evaluated by analyzing the clustering stability through 2 stability measures: the cell stability score and the coefficient of variation. Moreover, we confirmed clustering biological coherence by comparing tissue architecture with cluster shapes and by computing Moran's *I* to identify the spatial autocorrelated features. Method stability scores were compared with the ones achieved without using space to show how spatial information can significantly improve the clustering outcome. Results were also compared with those achieved by the state-of-the-art tools investigated, including *BayesSpace*, *SpaGCN*, *stLearn*, and *Giotto*. Results of each data set analysis assess that the proposed methods achieve more stable results with respect to clustering performed without considering spatial information and also that they are valid competitors, in terms of stability, to existing state-of-the-art clustering methods. Moreover, results demonstrated that the introduction of features from a histology image generally led to more unstable and misleading clustering results, particularly when the tissue section is quite uniform, and therefore, does not contain any particular structural information that could help clustering.

Additional Files

Figure S1: Spatial clusters plots in mouse kidney (MK) dataset. In (a) the results of 5 *Stardust* configurations with increasing space weight are shown. The same results, where only spots that have stability score >= 0.5 are visualized, are shown in (b). Each color corresponds to one of the 11, 9, 10, 10 and 10 cluster identities obtained in each configuration (in order of appearance), respectively.

Figure S2: Spatial clusters plots in human lymph node (HLN) dataset. In (a), the results of 5 *Stardust* configurations with increasing space weight are shown. The same results, where only spots that have stability score >= 0.5 are visualized, are shown in (b). Each color corresponds to one of the 14, 16, 19, 21 and 21 cluster identities obtained in each configuration (in order of appearance), respectively.

Figure S3: Spatial clusters plots in human heart (HH) dataset. In (a), the results of 5 *Stardust* configurations with increasing space weight are shown. The same results, where only spots that have stability score >= 0.5 are visualized, are shown in (b). Each color corresponds to one of the 13, 15, 14, and 15 cluster identities obtained in each configuration (in order of appearance), respectively.

Figure S4: Spatial clusters plots in human breast cancer (HBC1) dataset. In (a), the results of 5 *Stardust* configurations with increasing space weight are shown. The same results, where only spots that have stability score >= 0.5 are visualized, are shown in (b). Each color corresponds to one of the 14, 19, 17, 18 and 18 cluster identities obtained in each configuration (in order of appearance), respectively.

Figure S5: Spatial clusters plots in human breast cancer (HBC2) dataset. In (a), the results of 5 *Stardust* configurations with increasing space weight are shown. The same results, where only spots that have stability score >= 0.5 are visualized, are shown in (b). Each colour corresponds to one of the 14, 19, 20, 21 and 21 cluster identities obtained in each configuration (in order of appearance), respectively.

Figure S6: Spatial plots showing the expression level of three of the top 100 genes with highest Moran's index for HBC2, HH, HLN and MK Visium datasets and the clusters obtained with *Stardust**.

Figure S7: Comparison of *Stardust*, *Stardust** and state of art tools on HBC2 dataset: (a) The coefficient of variation values derived from the stability score distribution of each tool configuration. The cluster resolution refers to the resolution parameter for the Louvain community detection algorithm, image usage tells whether the image is included in the clustering method. (b) The cell stability score distributions of the best performing configuration of each tool (i.e., the one with the lowest coefficient of variation). (c) The H&E (Hematoxylin & Eosin) stained tissue sample and a spatial plot for each best tool configuration with clusters of spots on the tissue section. (d) The stability scores shifts obtained comparing the best configuration of each tool with the base *Stardust* no space version, i.e., the one not considering space.

Figure S8: Comparison of *Stardust* and *Stardust** and state of art tools on HH dataset. (a) The coefficient of variation values derived from the stability score distribution of each tool configuration. The cluster resolution refers to the resolution parameter for the Louvain community detection algorithm, image usage tells whether the image is included in the clustering method. (b) The cell stability score distributions of the best performing configuration of each tool (i.e., the one with the lowest coefficient of variation). (c) The H&E (Hematoxylin & Eosin) stained tissue sample and a spatial plot for each best tool configuration with clusters of spots on the tissue section. (d) The stability scores shifts obtained comparing the best configuration of each tool with the base *Stardust* no space version, i.e., the one not considering space.

Figure S9: Comparison of *Stardust*, and *Stardust** and state of art tools on HLN dataset. (a) The coefficient of variation values derived from the stability score distribution of each tool configuration. The cluster resolution refers to the resolution parameter for the Louvain community detection algorithm, image usage tells whether the image is included in the clustering method. (b) The cell stability score distributions of the best performing configuration of each tool (i.e.,

the one with the lowest coefficient of variation). (c) The H&E (Hematoxylin & Eosin) stained tissue sample and a spatial plot for each best tool configuration with clusters of spots on the tissue section. (d) The stability scores shifts obtained comparing the best configuration of each tool with the base *Stardust* no space version, i.e., the one not considering space.

Figure S10: Comparison of *Stardust*, *Stardust**, and state of art tools on MK dataset. (a) The coefficient of variation values derived from the stability score distribution of each tool configuration. The cluster resolution refers to the resolution parameter for the Louvain community detection algorithm, image usage tells whether the image is included in the clustering method. (b) The cell stability score distributions of the best performing configuration of each tool (i.e., the one with the lowest coefficient of variation). (c) The H&E (Hematoxylin & Eosin) stained tissue sample and a spatial plot for each best tool configuration with clusters of spots on the tissue section. (d) The stability scores shifts obtained comparing the best configuration of each tool with the base *Stardust* no space version, i.e., the one not considering space.

Figure S11: Time scalability of *Stardust* on five 10x datasets, two Seq-scope datasets and one Slide-seq dataset. Axes values are in the log10 scale.

Figure S12: Cluster Biological coherence. (a) Cell type annotation of Seq-scope Colon Tile 2110 dataset and clustering achieved using *Stardust** with cluster resolution 1.5 as in [21]. (b) Spatial plots showing the expression level of three of the top 100 genes with highest Moran's I for Seq-scope Colon Tile 2110 dataset.

Figure S13: Cluster Biological coherence. (a) Cell type annotation of Seq-scope Liver TD Tile 2117 dataset and clustering achieved using *Stardust** with cluster resolution 1 as in [18]. (b) Spatial plots showing the expression level of three of the top 100 genes with highest Moran's I for Seq-scope Liver TD Tile 2117 dataset.

Figure S14: Cluster Biological coherence. (a) Cell type annotation of Slide-seq cerebellum dataset and clustering achieved using *Stardust** with cluster resolution 0.6. (b) Spatial plots showing the expression level of three of the top 100 genes with highest Moran's I for Slide-seq cerebellum dataset.

Data Availability

- Project name: Stardust
- Project homepage: https://github.com/InfOmics/stardust/; rCASC is available on https://github.com/InfOmics/rCASC and GenSA for Stardust is available on https://github.com/SimoneAvesani/Tuning_Stardust.
- Operating system(s): UNIX-like OS (MacOS or a Linux distribution)
- Programming language: R
- Other requirements: Docker
- License: MIT license
- Any restrictions to use by nonacademics: None
- biotools: stardust
- RRID:SCR_022514

Availability of Supporting Data

The 10x data sets are available via the GitHub repository [25]. After registration on the 10x Genomics website [26], each individual data set can be downloaded from:

- Human breast cancer (HBC1): https://www.10xgenomics.com/resources/datasets/human-breast-cancer-block-a-section-1-1-standard-1-1-0
- Human breast cancer (HBC2): https://www.10xgenomics.com/resources/datasets/human-breast-cancer-block-a-section-2-1-standard-1-1-0
- Human heart (HH): https://www.10xgenomics.com/resources/datasets/human-heart-1-standard-1-1-0
- Human lymph node (HLN): https://www.10xgenomics.com/resources/datasets/human-lymph-node-1-standard-1-1-0
- Mouse kidney (MK): https://www.10xgenomics.com/resources/datasets/mouse-kidney-section-coronal-1-standard-1-1-0

Seq-scope data sets are available at the Deep Blue Data platform [27]

- Colon: https://deepblue.lib.umich.edu/data/downloads/rb68xc160
- Liver TD: https://deepblue.lib.umich.edu/data/downloads/7w62f844w

Slide-seq cerebellum data set is available, after registration, at the Broad Institute Single Cell Portal [28].

An archival copy of the code and supporting data are also available via the *GigaScience* repository, GigaDB [29].

Abbreviations

CSS: cell stability score; DCIS: ductal carcinoma in situ; GenSA: Generalized Simulated Annealing; HBC1: human breast cancer 1; HBC2: human breast cancer 2; HH: human heart; HLN: human lymph node; HMRF: hidden Markov random field; MK: mouse kidney; PC: principal component; PCA: principal component analysis; rCASC: reproducible Classification Analysis of Single Cell Sequencing Data; RDS: R data serialized; scRNA-seq: single-cell RNA sequencing; ST: spatial transcriptomics.

Author Contributions

Conceptualization: RG and GM; Methodology: RG, SA, EV, LA, GM, VB, MB, RC; Supervision: RG, RC; Writing: RG, SA, EV; Review & editing: all; Code writing: SA, EV, LA, GM; Test: SA, EV; Validation: RG, SA, EV, RC. None of the authors have any competing interests in the manuscript.

Acknowledgments

We thank Prof. Giorgio Cattoretti for the useful comments and discussions on the paper.

References

1. Buettner, F, Natarajan, KN, Casale, FP, *et al.* Computational analysis of cell-to-cell heterogeneity in single-cell RNA-sequencing data reveals hidden subpopulations of cells. *Nat Biotechnol* 2015;**33**(2):155–60.
2. Lewis, SM, Asselin-Labat, ML, Nguyen, Q, *et al.* Spatial omics and multiplexed imaging to explore cancer biology. *Nat Methods* 2021;**18**(9):1–16.
3. Ståhl, PL, Salmén, F, Vickovic, S, *et al.* Visualization and analysis of gene expression in tissue sections by spatial transcriptomics. *Science* 2016;**353**(6294):78–82.

4. Asp, M, Bergenstråhle, J, Lundeberg, J. Spatially resolved transcriptomes—next generation tools for tissue exploration. *Bioessays* 2020;**42**(10):1900221.
5. Marx, V. Method of the year: spatially resolved transcriptomics. *Nat Methods* 2021;**18**(1):9–14.
6. Rao, A, Barkley, D, França, GS, *et al.* Exploring tissue architecture using spatial transcriptomics. *Nature* 2021;**596**(7871):211–20.
7. Hu, J, Schroeder, A, Coleman, K, *et al.* Statistical and machine learning methods for spatially resolved transcriptomics with histology. *Computational Structural Biotechnol J* 2021;**19**:3829.
8. Xu, Y, McCord, RP. CoSTA: unsupervised convolutional neural network learning for spatial transcriptomics analysis. *bioRxiv* 2021.
9. Teng, H, Yuan, Y, Bar-Joseph, Z. Clustering spatial transcriptomics data. *Bioinformatics* 2021;**38**(4):997–1004.
10. He, Y, Tang, X, Huang, J, *et al.* ClusterMap for multi-scale clustering analysis of spatial gene expression. *Nat Commun* 2021;**12**(1):1–13.
11. Pham, D, Tan, X, Xu, J, *et al.* stLearn: integrating spatial location, tissue morphology and gene expression to find cell types, cell-cell interactions and spatial trajectories within undissociated tissues. *bioRxiv* 2020.
12. Hu, J, Li, X, Coleman, K, *et al.* Integrating gene expression, spatial location and histology to identify spatial domains and spatially variable genes by graph convolutional network. *bioRxiv* 2020.
13. Dries, R, Zhu, Q, Dong, R, *et al.* Giotto: a toolbox for integrative analysis and visualization of spatial expression data. *Genome Biol* 2021;**22**(1):1–31.
14. Zhao, E, Stone, MR, Ren, X, *et al.* Spatial transcriptomics at subspot resolution with BayesSpace. *Nat Biotechnol* 2021;**39**(11):1–10.
15. Butler, A, Hoffman, P, Smibert, P, *et al.* Integrating single-cell transcriptomic data across different conditions, technologies, and species. *Nat Biotechnol* 2018;**36**(5):411–20.
16. Human Breast Cancer (Block A Section 1), Human Breast Cancer (Block A Section 2), Human Heart, Human Lymph Node, Mouse Kidney Section (Coronal), Spatial Gene Expression by Space Ranger 1.1.0, 10x Genomics. [accessed 2020 Jun 23]. https://support.10xgenomics.com/docs/citations.
17. Cho, CS, Xi, J, Si, Y, *et al.* Microscopic examination of spatial transcriptome using Seq-Scope. *Cell* 2021;**184**(13):3559–3572.e22.
18. Cable, DM, Murray, E, Zou, LS, *et al.* Robust decomposition of cell type mixtures in spatial transcriptomics. *Nat Biotechnol* 2022;**40**(4):1–10.
19. Alessandrì, L, Cordero, F, Beccuti, M, *et al.* rCASC: reproducible classification analysis of single-cell sequencing data. *Gigascience* 2019;**8**(9):giz105.
20. Stuart, T, Butler, A, Hoffman, P, *et al.* Comprehensive integration of single-cell data. *Cell* 2019;**177**(7):1888–1902.e21.
21. Cho, C-S, Xi, J, Kang, HM, *et al. Seq-Scope processed datasets for liver and colon results (RDS) and H&E images [Data set]*. University of Michigan—Deep Blue Data. 2021. https://doi.org/10.7302/cjfe-wa35.
22. Blondel, VD, Guillaume, JL, Lambiotte, R, *et al.* Fast unfolding of communities in large networks. *J Stat Mech Theory Exp* 2008;**2008**(10):P10008.
23. Jolliffe, IT, Cadima, J. Principal component analysis: a review and recent developments. *Philos Trans R Soc A* 2016;**374**(2065):20150202.
24. Xiang, Y, Gubian, S, Suomela, B, *et al.* Generalized simulated annealing for global optimization: the GenSA package. *R J* 2013;**5**(1):13.
25. Stardust. GitHub repository. [accessed 2022 Apr 24]. https://github.com/InfOmics/stardust/.
26. 10X Genomics Ressources. [accessed 2021 Jan 25]. https://www.10xgenomics.com/resources/datasets.
27. Deep Blue Data platform. [accessed 2022 Apr 15]. https://deepblue.lib.umich.edu/data/concern/data_sets/9c67wn05f?locale=en.
28. Broad Institute Single Cell Portal. [accessed 2022 Apr 15]. https://singlecell.broadinstitute.org/single_cell/study/SCP948.
29. Avesani, S, Viesi, E, Alessandrì, L, *et al.* Supporting data for "Stardust: improving spatial transcriptomics data analysis through space aware modularity optimization based clustering." *GigaScience Database*. 2022. http://dx.doi.org/10.5524/102224.